Microtopography obtained through UAV surveys for active tectonic studies

Rui Afonso Caldas Canedo Mateus Marques

September 2021

Abstract

The main objective of this work was – using very high spatial resolution data captured by UAV – to generate point clouds and digital terrain models that were free from surface vegetation.

From three-dimensional treated models whose vegetation presence was minimized as much as possible, it was hypothesized if this combination of [technology + methodology] could detect the presence of geological faults that were already known to exist.

This hypothetical detection was based on filters whose accuracy depended directly, not only on the quality of the images obtained, but also on the quality of the "vegetation" category classification.

All images were obtained in the Tagus River Valley. This was due to being a location in which there is known to exist geological activity and because there was the possibility of collaborating with an ongoing project; (Heleno, Pina, Bandeira, Vilanova, & Goyanes, ALTITUD3 - Assessment of Low-cost Aerial Intelligent systems for natural Terrain 3D mapping, s.d.):

- ALTITUD3 – Assessment of Low-cost Aerial Intelligent systems for natural Terrain 3D mapping.

This projects main focus is establishing protocols for the acquisition of images using UAV and the improvement of image processing methods that enable obtaining point clouds that make possible the production of high detail three-dimensional models. Thankfully, it provided 100% of the data used in this master thesis.

Keywords: Tectonic; UAV; Structure from Motion; DEM; Watershed; Angular alignment.

1. Introduction

This master thesis is focused on the applicability of an emerging, non-intrusive technology in the detailed study of tectonic structures. Using sensors coupled to unmanned aerial vehicles, from now on called "UAV", three-dimensional digital models of surface and terrain were obtained with resolutions far superior to all the previous ones obtained with other techniques.

These three-dimensional digital models arose from the use of two typical software from this domain of practical application: METASHAPE (Agisoft LLC) and ENVI (L3Harris Geospatial). The results are mathematical representations and digital descriptions with much more detail of the observed physical world. In addition, an

attempt was made to develop a method that would allow the correct classification and consequent distinction between the so--called "ground points" and "vegetation points" (uninteresting points that *mask* the ground surface and that should not be considered).

After the classification, each of the categories owed its name, ideally, to the portion of soil/vegetation that, in the physical world, was captured by the sensor used and was, in fact, either “soil” or” vegetation” – so that they could be placed in each of the respective categories.

This separation arose from an optimization process of several methods of classification and point filtering.

This work is highly relevant because studying, analysing, and understanding terrestrial tectonics is directly contributing to the understanding of our planet and its habitability. Accurate identification of the types of structures and their boundary locations over time is essential to understand the evolution of the plate/mantle system. It is from the transformation of material between the different, deepest, environments that the terrestrial surface, as we know it, emerges.

Thus, this dissertation sought to answer the question: "Can UAV be used to evidence/predict the occurrence of tectonic phenomena by detecting their repercussions on the earth's surface?"

2. Data

All the work was centred in a set of 15 (from 659) photographs taken with a UAV in an uncrossed flight with an overlap greater than 90%. From the spatial alignment of all the images collected, the processing base is obtained, it is composed by the set of images that, being placed in the right place in terms of adjacency, allow the software to apply computational methods and algorithms based on Structure from Motion – SfM – and the search for "common points" to generate Clouds of points.

Next, in the Picture 2:1 there is a graphical representation of the various images that gave rise to the *sparse cloud*: it contains an example of what is presented in AGISOFT METASHAPE at the beginning of the Processing phase.

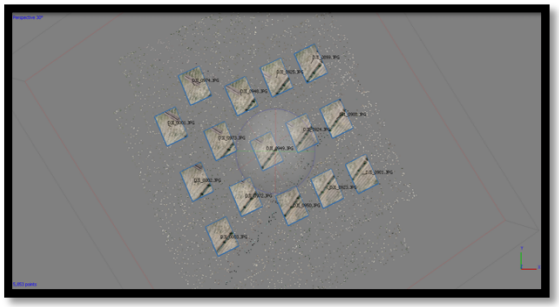

Picture 1:1 - Screenshot from AGISOFT.

This moment marks the passage from the practical domain centred on UAV to the practical domain centred on software, in which most of the methodology was developed.

3. Methodology

The processing phase is where the biggest portion of the methodology occurs, it represents the central point of this work, all processing focused on developing a method consisting in tests and improvements in a point cloud (product of the alignment of the 15 images) from a portion of the initial area in which a ditch of dimensions A x B x C [m^3] was excavated.

Below – Picture 3:1 – a scheme of the chronology of the steps that were given, as well as the main objective of each step.

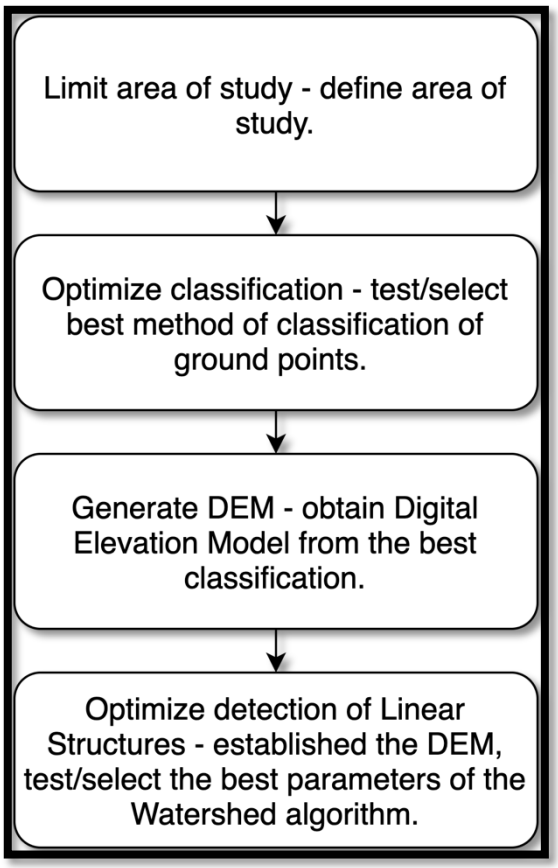

Picture 3:1 - Chronology of methodology.

Although all the steps in this 3rd chapter produced visual outputs, those outputs are only sub products of one ongoing process of optimization. That said, they are not actual results. Those sub products are images that only exist in the halfway paths of optimization.

Next it will be presented each one of the phases as well as the most significant outputs of each phase.

Area of study

The part where the area of study was defined consisted of selecting the images where the ditch was clearly visible, the "output" of this first part were the 15 images (from 659) selected as the main subject of the analysis and shown in the previous chapter on the Picture 2:1.

Classification of Ground Points

The main part of the developed methodology occurred during the optimization phases: Optimize Classification and Optimize detection of Linear Structures.

To obtain ground points, first we had to Classify them, and that could be made using two methods:

- Parametric Classification
- Supervised Classification.

Parametric classification

Through the parametric classification, it was necessary to choose the values to be assigned to the three basic parameters: a-Cell Size; b-Max. Distance; c-Max. Angle.

The approach was, always based on the knowledge of the actual terrain, to set three limits: 3-upper; 2-intermediate; and 1-lower. For each of the two -b and c- parameters to be optimized; because a-Cell Size had a fixed value... (Visual representation of the parametric Classification table below – Picture 3:2 –)

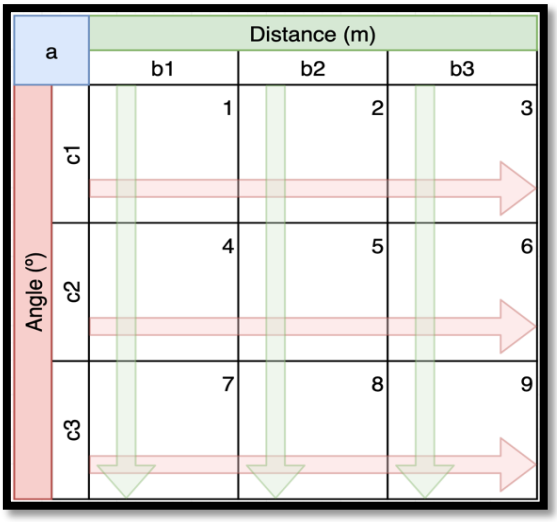

Picture 3:2 - Parametric Classification table.

…Through a double-entry table, it was possible to evaluate not only the 9 (=3^2) classification results, but also understand in which direction of parameter variation the most satisfactory results were obtained. And given that direction of improvements, try to generate halfway pictures to really understand if the ones we had initially could be improved with some sub-set of parameters not present in the first 3x3 matrix.

The outputs of this part were the 11 images (9 obtained corresponding to the previous matrix and 2 more that were intermediate states of even more refined optimization try--outs) much alike the picture below – Picture 3:3. Once reached a point where no better

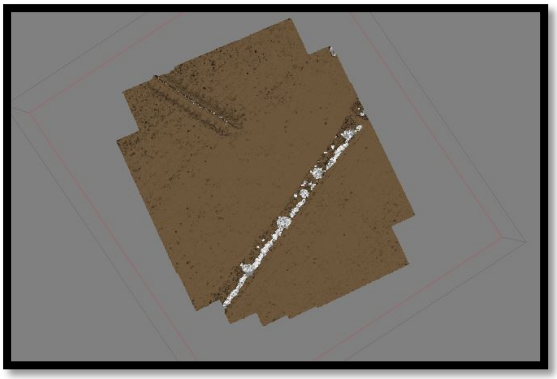

Picture 3:3 - Parametric Classification example.

images could be generated, the optimization process of the Parametric Classification was stopped, and the best image was kept until further developments.

Supervised Classification

After, to test the other classification method – Supervised – the focus was obtaining ground points through a Supervised Classification. To successfully conclude this classification, the user must define two inputs:

1) Colour – total of 12 categories used in this work. 3 from a-vegetation; 3 from b-soil; 3 from c-trees and 3 from d-ditch.
2) Tolerance – total of 3 tolerance values used.

From the combination of these two choices, the attribution of a class arises. To better understand what the above-mentioned choices correspond to; the following example is presented:

Given a photographic representation of the aerial study area, if you want to classify "trees", you can select a "green" dot that is part of a tree in the image under analysis and stipulate a tolerance of $\varkappa$*. Then the software will return a set of dots that 1) are "green"; 2) are "*$\varkappa$ *%" around the shade (of green) of the point that served as a sample. There, the user can categorize them as "tree".*

It was, therefore, crucial to understand for which tolerance values, one could obtain more satisfactory colour point selections so that classes could be assigned to each of these colour selections/sets under analysis. Classes always originate in the colours of the image to be classified and categorized.

So, the process consisted in, running through a cycle of attributing 12 categories (Picture 3:4, below) for each one of the 3

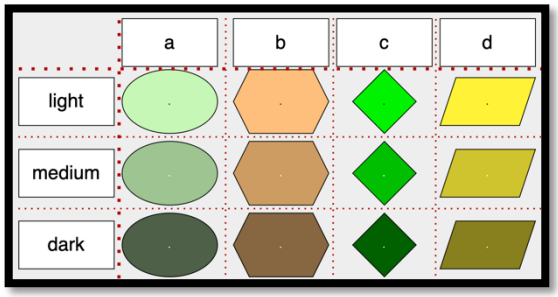

Picture 3:4 - Visual representation of the 12 categories.

fixed tolerances.

A total of 3 cycles were made, one for each one of the three values [10%; 20%; 30%] of Tolerance established.

The output of this part were 3 final images (one of them, below – Picture 3:5), each one corresponding to a pre-established value of %tolerance:

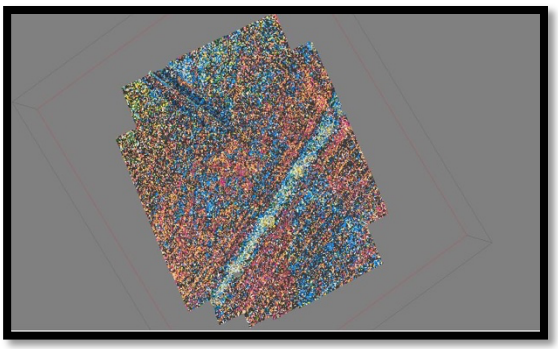

Picture 3:5 - Supervised Classification example.

Once finalized the classification process, it was time to evaluate the DEM obtained from each of the best classification.

Obtaining DEM

From each of the best results of each of the classifications resulted a Digital Elevation Model (exemplified below, on Picture 3:6), these were visually evaluated in the software through the representation of points that were later compared with what was observed on the field.

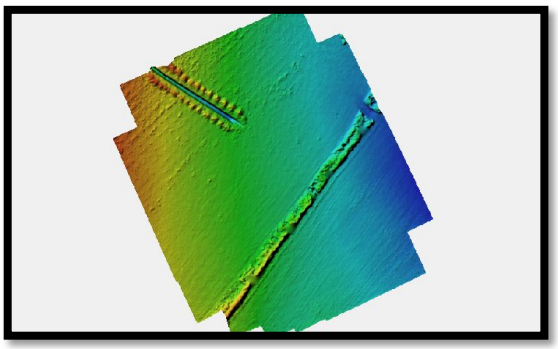

Picture 3:7 - Digital Elevation Model.

Detection of Linear Structures

The filtering part of DEM takes place in another Software: ENVI. In this phase, an attempt was made to obtain an extraction of linear elements/structures, limiting them by segments.

The function used was Feature Extraction – Segments Only. This software function has as its central point the Watershed algorithm and through the optimization of two more parameters – Scale and Merge – it allows to generate shapes of segments without having to perform a classification based on spatial rules (such as parametric) or in examples (such as supervised).

• Watershed: is an algorithm that originated in the 1980s (Beucher, 2000), treating images as topographic maps, whose basic principle is the formation of basins, having as its final output "regions". See below, the Picture 3:7; It contains a simple example of the type of regions the software can generate from a given topographic map.

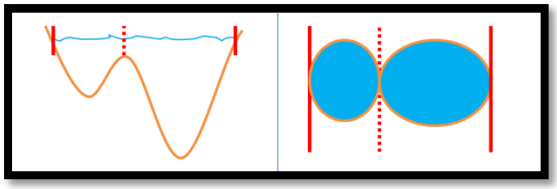

Picture 3:6 - Left-Topographic representation; Right-Region generated.

In the practical case discussed, we seek to evidence the possible existence of a failure, so, once again, as shown in Picture 3:8, the two parameters – Merge and Scale – were

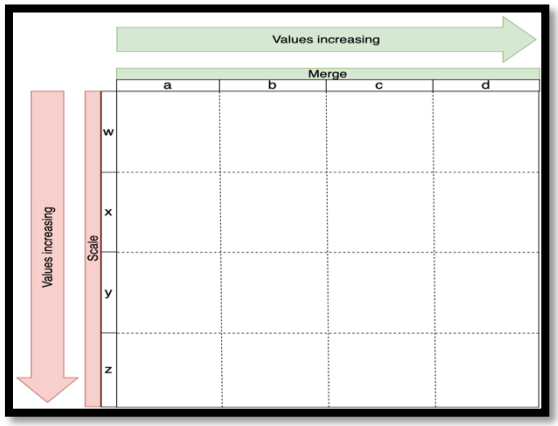

Picture 3:8 - Merge / Scale matrix.

optimized through a double-entry table

generating 16 (4x4) output images, the knowledge of the terrain and geomorphology associated with the aim of this work led us to predict/explain the results obtained. The way the values were used for each of these parameters being [a; b; c; d] for Merge and [w; x; y; z] for Scale are exemplified in the previous scheme.

The outputs of this part were 18 (16 + 2) filtered images like the one below, Picture 3:9; 16 corresponding to the previous matrix and 2 more corresponding to extra trials.

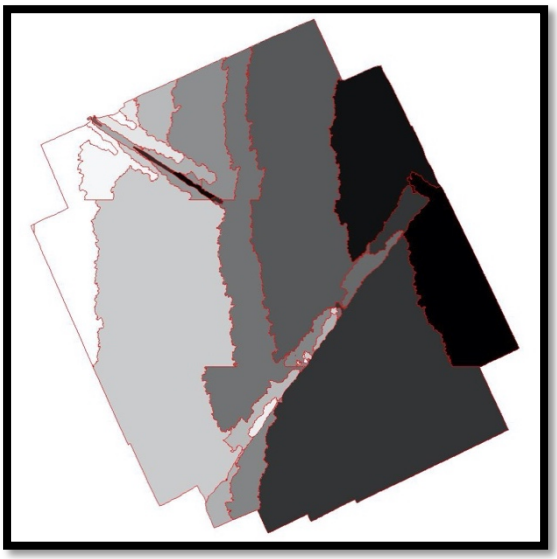

Picture 3:10 - Filtered image after Merge + Scale.

4. Results

Once the methodology was concluded and all the optimizations possible within the timespan available had taken place only remained, finally, to make a comparative analysis between the expected alignment between the fault known to exist (and marked *in loco*) with the apparent alignment of the linear structures (or shapes) that emerged in the previous steps. The real fault alignment is shown next on the Picture 4:1.

From the eventual alignment between the real azimuths – observed on the spot – and the expected ones – dictated by the watershed segmentation algorithm – some

Picture 3:9 - Orientation of the real direction of the fault.

conclusions could be drawn. The two images that are presented below (Pictures 4:2 and 4:3) show this comparison.

In the first, its illustrated what's the actual alignment of the fault as well as part of the filtering (irregular yellow lines) obtained.

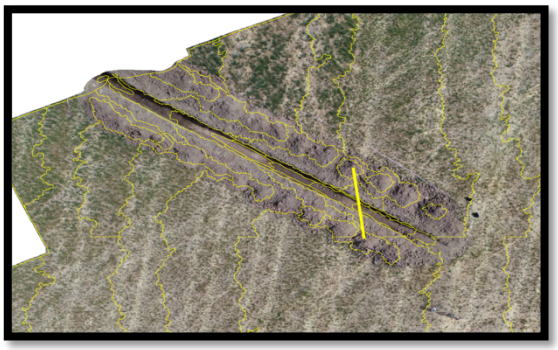

Picture 4:1 - Real direction + filters.

In a second part, using a simple superposition of straight lines, parallel to

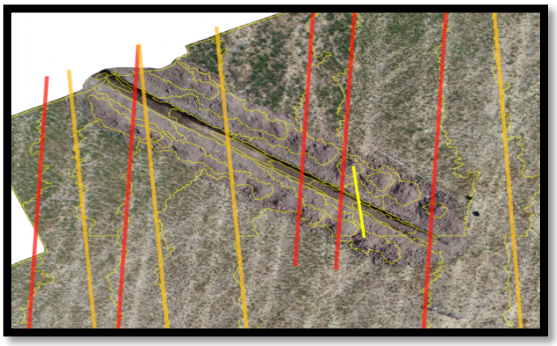

Picture 4:2 - Two families based on predominant filter directions.

each other, two families of possible "predictable" failures were identified by the method and algorithm.

Finally, seeking to reinforce confidence in the method used, through the possible coincidence of the results obtained by computer with the reality observed; the angles of the families were measured, and their angular deviations compared to reality.

Thus, the basis of reasoning that precedes the conclusions becomes evident: The maximum angular deviation (worst result) possible to observe is 90º. This would correspond to the prediction given by the method being perpendicular to the failure observed *in loco*. Therefore, it is assumed that 90º of deviation between the real value and a value given by the method corresponds to the maximum error possible to observe – 100% error. And so, the formula to obtain this percentage of error compared to the total; is simply the ratio between the absolute value of the difference between the angles and the maximum allowable difference in this case, that is:

$$\%Error = \frac{|Real\ reference - Method\ reference|}{Max\ deviation - Min\ deviation}.100$$

Two families with angles of 94º (red) and 84º (dark yellow) were observed. Establishing as the "Real reference" value the real angle of the fault – 81º – and assuming a direct proportionality between the factor "angular deviation" and the factor "percentage of error"; the results of applying this method indicate errors (%) expected from:

$$\%\boldsymbol{Error\ of\ Red\ Family} = \frac{|81 - 94|}{90 - 0}.100 = \mathbf{14,4}$$

$$\%\boldsymbol{Error\ of\ Dark\ Yellow\ Family} = \frac{|81 - 84|}{90 - 0}.100 = \mathbf{3,3}$$

In summary: UAV were used to capture images; these images were converted into three-dimensional clouds of points from which, through different classifications, the pixels corresponding to the vegetation were extracted/excluded. Then, DEM were generated which were filtered to obtain linear structures, and finally, these linear structures seem to indicate the presence of two different families of alignments; one of which "mistakes" in its orientation only by 3 degrees which corresponds to a percentage of 3.3 compared to the maximum value possible to be observed in any circumstance.

5. Conclusions

This dissertation had as its central point the hypothesis of using UAV as a mean of detection of microtopography, in this case specifically as a mean of deduction and/or prediction of geological faults through the identification of linear structures. In fact, if much of the work was image processing and parameter optimization... this would never yield minimally plausible results if the initial acquisition did not provide at least reasonable digital support so that the entire methodology could be applied.

It can always, as in any hypothesis testing process, be said that any coincidence between the results obtained and reality was just that, a coincidence. In this specific case, since we had factual data on the existence of the fault and more, on its real alignment, it is a coincidence that very much reinforces the validity of the developed methodology.

It was never the objective of this dissertation to affirm the existence of an infallible method, it was, rather, to test the hypothesis that UAV can be an economically viable tool or alternative for obtaining and analyzing microtopography and this is clearly evidenced not just by the variety of tests that could be done with the initial data, but also by the confidence conveyed by the very low margins of error at the end.

We then return to the question initially stated: “Can UAV be used to evidence/predict the occurrence of tectonic phenomena by detecting their repercussions on the earth's surface?”

- Most probably yes. It is undeniable that, in this case, microtopographic patterns were evidenced and that these have a strong relationship with the occurrence of tectonic phenomena. However, there is no absolute certainty that everything is not just circumstantial. In short, the only way to gain more and more confidence that the results obtained by applying this type of methodology are positive is just to repeat the process enough times until the results are systematically observed to coincide with reality.

6. Bibliography

Beucher, S. (2000, Julho). The Watershed Transformation Applied To Image Segmentation. *Scanning microscopy Supplement 6*, pp. 1-26.

Canora, C., Vilanova, S., De Pro-Diáz, Y., Pina, P., & Heleno, S. (2021, March). Evidence of Surface Rupture Associated With Historical Earthquakes in the Lower Tagus Valley, Portugal. Implications for Seismic Hazard in the Greater Lisbon Area. *Frontiers in Earth Science*, p. Article 620778.

Chen, J., Li, K., Chang, K.-J., Sofia, G., & Tarolli, P. (October de 2015). Open-pit mining geomorphic feature characterisation. *International Journal of Applied Earth Observation and Geoinformation, XLII*, pp. 76-86.

Eltner, A., Kaiser, A., Castillo, C., Rock, G., Neugirg, F., & Abellán, A. (2016, May). Image-based surface reconstruction in geomorphometry – merits, limits and developments. *European Geosciences Union*.

F.L.Bonali, A.Tibaldi, F.Marchese, L.Fallati, E.Russo, C.Corselli, & A.Savini. (2019, April). UAV-based surveying in volcano-tectonics: An example from the Iceland rift. *Journal of Structural Geology*.

Gori, S., Falcucci, E., Galadini, F., Zimmaro, P., Pizzi, A., Kayen, R. E., . . . Stewart, J. P. (2019, December). Surface Faulting Caused by the 2016 Central Italy Seismic Sequence: Field Mapping and LiDAR/UAV Imaging. *SAGE Journals*.

Hader, M., & Baur, S. (2020). *USD 5.5 billion market volume for non-military drones globally.* Roland Berger.

Heleno, S., Pina, P., Bandeira, L., Vilanova, S. P., & Goyanes, G. A. (n.d.). *ALTITUD3 - Assessment of Low-cost Aerial Intelligent systems for natural Terrain 3D mapping*. Retrieved Fevereiro 2021, from Cerena - Centro de Recursos Naturais e Ambiente: https://cerena.ist.utl.pt/projects/altitud3-assessment-low-cost-aerial-intelligent-systems-natural-terrain-3d-mapping

Heleno, S., Pina, P., Bandeira, L., Vilanova, S., & Goyanes, G. A. (October 1st 2018-On going). *ALTITUD3 - Assessment of Low-cost Aerial Intelligent systems for natural Terrain 3D mapping.* Fundação para a Ciência e a Tecnologia.

Humboldt State University. (2017). Learning Module 8.2 - UAS and the Future of Remote Sensing. *Introduction to Remote Sensing*.

Iglhaut, J., Cabo, C., Puliti, S., Piermattei, L., O'Connor, J., & Rosette, J. (2019, Julho). Structure from Motion Photogrammetry in Forestry: a Review. *Springer - Part of a collection: Topical Collection on "Remote Sensing"*.

Javernick L., B. J. (2014, May). Modeling the topography of shallow braided rivers using Structure-from-Motion photogrammetry. *Geomorphology*, pp. 166-182.

Kadhim, I., & Abed, F. M. (2021, January). The Potential of LiDAR and UAV-Photogrammetric Data Analysis to Interpret Archaeological Sites: A Case Study of Chun Castle in South-West England. *MDPI*.

Lian, X.-g., Li, Z.-j., Yuan, H.-y., Liu, J.-b., Zhang, Y.-j., Liu, X.-y., & Wu, Y.-r. (2020). Rapid identification of landslide, collapse and crack based on low-altitude remote sensing image of UAV. *Journal of Mountain Science*.

Lucieer, A., de Jong, S. M., & Turner, D. (2014, February). Mapping landslide displacements using Structure from Motion (SfM) and image correlation of multitemporal UAV photography. *Progress in Physical Geography-Earth and Environment, XXXVIII*(1), pp. 97-116.

Measure. (2016). *Drones: Autonomous or automated?* Obtained February 5th 2021, from https://www.measure.com/blog/drones-autonomous-or-automated#:~:text=Currently%2C%20drones%20cannot%20perform%20all,they%20are%2C%20however%2C%20automated.

Nex, F., & Remondino, F. (November 2013). UAV for 3D mapping applications: a review. *Applied Geomatics,6*.

Olson, D., & Anderson, J. (2021, January). Review on unmanned aerial vehicles, remote sensors, imagery processing,

and their applications in agriculture. *Agronomy Journal*.

Park, S., & Choi, Y. (2020, July). Applications of Unmanned Aerial Vehicles in Mining from Exploration to Reclamation: A Review. *MDPI - Minerals*.

Scientific Volume Imaging - Watershed Segmentation - Explanation. (n.d.). *Deconvolution - Visualization - Analysis*. Retrieved from www.svi.nl/watershed

Sledź, S., Ewertowski, M., & Piekarczyk, J. (2021, January). Applications of unmanned aerial vehicle (UAV) surveys and Structure from Motion photogrammetry in glacial and periglacial geomorphology.

Spring, K. R., Flynn, B. O., Long, J. C., & Davidson, M. W. (n.d.). *Spatial Resolution in Digital Imaging*. Retrieved February 5th, 2021, from https://www.microscopyu.com/tutorials/spatial-resolution-in-digital-imaging

Török, A., Bögöly, G., Somogyi, Á., & Lovas, T. (2020, January). Application of UAV in Topographic Modelling and Structural Geological Mapping of Quarries and Their Surroundings—Delineation of Fault-Bordered Raw Material Reserves. *MDPI*.

Tahir, A., Boling, J., Haghbayan, M.-H., Toivonen, H., & Plosila, J. (December 2019). Swarms of Unmanned Aerial Vehicles - A Survey. *Journal of Industrial Information Integration, XVI*.

Ulman, S. (1976). *dspace.* Retrieved from https://dspace.mit.edu/bitstream/1721.1/6298/2/AIM-476.pdf

Xiong, B., & Li, X. (2020, July). Offset measurements along active faults based on the structure from motion method – A case study of Gebiling in the Xorkoli section of the Altyn Tagh Fault. *Geodesy and Geodynamics*.